Available online at BCREC website: https://bcrec.id

Bulletin of Chemical Reaction Engineering & Catalysis, 17 (3) 2022, 638-649

Research Article

Nickel Supported Parangtritis Beach Sand (PP) Catalyst for Hydrocracking of Palm and Malapari Oil into Biofuel

Muh. Siddik Ibrahim, Wega Trisunaryanti*, T. Triyono

Department of Chemistry, Universitas Gadjah Mada, Yogyakarta, Indonesia.

Received: 25th August 2022; Revised: 22nd September 2022; Accepted: 23rd September 2022
Available online: 24th September 2022; Published regularly: September 2022

Abstract

Nickel supported Parangtritis beach sand (PP) catalyst for hydrocracking of palm and malapari oil into biofuel has been conducted. The impregnation process of Nickel (Ni) metal on PP was carried out through the dry impregnation method (blending) using a precursor salt of $NiCl_2.6H_2O$ with variations of Ni metal as much as 10 and 20 wt% of PP which produced Ni(A) and Ni(B) catalysts. Each catalyst was tested for activity and selectivity through the hydrocracking process of oil into biofuel using a semi-batch system reactor at a temperature of 450 °C, a hydrogen gas flow rate of 20 mL/minute for 2 hours, and a weight ratio of 1:200 catalyst:feed (w/w). The results showed that the Ni(A)/PP catalyst had the highest activity and selectivity with the yield of liquid products and the total biofuel fraction (biohydrocarbons) obtained from hydrocracking of palm oil of 68.50 and 49.87 wt%, respectively. Ni(A)/PP catalyst has a total acidity, surface area, and crystal size of 0.051 mmol/g, 4.44 m^2/g, 25.86 nm, respectively. The reusability test of the Ni(A)/PP catalyst in the hydrocracking process of palm oil into biofuel after the third use resulted in a liquid product and the total biofuel fraction obtained was 64.20 and 41.46 wt%, respectively. The yield of liquid product and the total fraction of biofuel (biohydrocarbon) in hydrocracking malapari oil were 66.10, 47.83 wt%, respectively.

Keywords: Parangtritis beach sand; nickel; hydrocracking; vegetable oil

How to Cite: M.S. Ibrahim, W. Trisunaryanti, T. Triyono. (2022) Nickel Supported Parangtritis Beach Sand (PP) Catalyst for Hydrocracking of Palm and Malapari Oil into Biofuel. *Bulletin of Chemical Reaction Engineering & Catalysis*, 17(3), 638-649 (doi: 10.9767/bcrec.17.3.15668.638-649)

Permalink/DOI: https://doi.org/10.9767/bcrec.17.3.15668.638-649

1. Introduction

Oil and gas are natural resources that contribute significantly to human life. Along with the growth of the human population, its vital role and utilization as fuel will continue to expand. However, the energy used today is nonrenewable and derived from petroleum. On the other hand, population, industry, and transportation continue to grow over time, resulting in a rising demand for fuel oil. If this continues, a fuel shortage will ensue. This has prompted research into the discovery of alternative renewable fuels, one of which is converting vegetable oils like palm oil and malapari into biofuels.

Utilizing Indonesia's abundant vegetable oil for fuel production can solve the problem of the availability of renewable fuel sources [1]. In addition, producing biofuels from vegetable oils can reduce reliance on fossil fuels and their associated greenhouse gas emissions [2]. Many different chemical compositions are present in fatty acids found in vegetable oils like palm and malapari, which can be processed into biofuel fractions [3]. Thermal cracking is one possible method for converting vegetable oil into biofuel.

* Corresponding Author.
Email: wegats@ugm.ac.id (W. Trisunaryanti)

However, over cracking typically occurs during thermal cracking, resulting in the production of low-quality coke, gas, and naphtha [4]. This may result in a decrease in the quantity of the desired product. In order to optimize the production of the desired product, a catalyst is added to the hydrocracking process, which is currently known as the catalytic hydrocracking process, during the cracking process.

In addition to being a simple method, catalytic hydrocracking is more cost-effective, and most importantly, the fuel produced by the catalytic hydrocracking process has the same chemical composition as fossil fuels [5]. This research utilizes Ni metal as the catalyst material and Parangtritis beach sand as the carrier. Numerous studies on catalysts derived from beach sand have been conducted because of the silica-rich nature of beach sand [6,7] for hydrocracking of used palm oil into hydrocarbon compounds. The liquid product and total hydrocarbon compounds obtained were 69.75 and 94.33 wt%, respectively.

In addition to its abundant availability, Parangtritis beach sand possesses enormous potential for use as a catalyst carrier without the need for extraction. Because fewer chemical reagents are required to prepare catalyst materials, this is an interesting and useful discussion if it is conducted with an eye toward the environment. Even economically, Parangtritis beach sand is less expensive or free compared to synthetic porous materials such as MCM-41, Al_2O_3, ZSM-5, etc., which must be purchased for a cost. Therefore, this study aims to observe the properties, activity, selectivity, and reusability of metal catalysts supported Parangtritis beach sand on hydrocracking of palm and malapari oil into biofuel.

2. Materials and Methods

2.1. Materials

Parangtritis beach sand was collected in Yogyakarta, nickel chloride hexahydrate ($NiCl_2.6H_2O$, 99.9%), pyridine (C_5H_5N, 99.5%) from Merck & Co., nitrogen gas (N_2), technical hydrogen gas (H_2) from PT. Samator Gas, palm and malapari oil.

2.2. Preparation of Parangtritis Beach Sand

The sand was washed with distilled water before being dried in a 100 °C oven for 24 hours. The sand was then ground into fine particles using a ball mill, calcined at 500 °C for 5 hours with N_2 gas flow, reduced at 450 °C for 3 hours with H_2 gas flow, and filtered through a 100-mesh sieve. The sand that has been filtered is then known as PP.

2.3. Impregnation of Metals into Parangtritis Beach Sand (PP)

The dry impregnation method was used to impregnate Nickel (Ni) metal onto beach sand (PP) using $NiCl_2.6H_2O$ precursor salt with loadings of 10 and 20% Ni metal by weight of PP, denoted as Ni(A)/PP and Ni(B)/PP, respectively. The precursor salt and 4 g of PP were blended for 15 minutes in a ball mill. After that, the Ni/PP mixture was calcined at 500 °C for 5 hours at a flow rate of 20 mL/min using nitrogen gas. This procedure was followed by a 3-hour hydrogen gas reduction at 450 °C and 20 mL/min.

2.4. Catalyst Characterization

PP, Ni(A)/PP, and Ni(B)/PP catalysts were characterized using Fourier-Transform Infra-Red (FT-IR, SHIMADZU Prestige 21) to analyze functional groups, Gas Sorption Analyzer (GSA, Quantachrome TouchWin version 1.11) to determine the surface area. Meanwhile, pore volume and pore diameter were measured using the Brunauer-Emmet-Teller (BET) and Barrett-Joyner-Halenda (BJH) methods. Other characterizations performed were X-Ray Diffraction (XRD, Bruker D2 Phaset 2 Gen) to determine the crystallinity of the catalyst, Scanning Electron Microscope (SEM-EDX, JEOL JSM-6510) to see the surface morphology, Transmission Electron Microscope (JEOL-JEM-1400) to see the catalyst pore morphology, and acidity test using pyridine base adsorption gravimetric method.

2.5. Catalyst Activity Test

The catalytic activity test was conducted through the palm oil hydrocracking process. PP, Ni(A)/PP, and Ni(B)/PP catalysts derived from the preparation process were tested using a weight ratio of 1/200 (wt%) of the palm oil catalyst/feed used. Hydrocracking was performed in a stainless-steel semi-batch reactor at a temperature of 450 °C for 2 hours using hydrogen gas at a flow rate of 20 mL/min. The catalyst with the highest activity and selectivity in producing liquid products and biofuel fractions will be further used in the hydrocracking process of malapari oil. In addition, the reusability of the hydrocracking catalyst will be tested for 3 continuous runs using a used catalyst. The liquid product obtained from hydrocracking was analyzed using Gas Chro-

matography-Mass Spectrometry (GC-MS) to determine the compound content in the liquid product. The hydrocracking product distribution can be calculated using the following equations:

$$Liquid\ product\ conversion\ (wt\%) = \frac{liquid\ product\ weight}{feed\ weight} x100\% \quad (1)$$

$$Coke\ conversion\ (wt\%) = \frac{(weight\ to\ final\ cat. - weight\ of\ initial\ cat.)}{feed\ weight} x100\% \quad (2)$$

$$Residual\ conv.\ (wt\%) = \frac{(final\ feed\ container\ weight - empty\ container\ weight)}{feed\ weight} x100\% \quad (3)$$

$$Gas\ conversion\ (wt\%) = 100\% - (liquid + coke + residue\ conv.) \quad (4)$$

$$Gasoline\ fraction = \frac{\%compound\ area\ C5 - C12}{Total\ \%area} xLiquid\ product\ (wt\%) \quad (5)$$

$$Avtur\ fraction = \frac{\%compound\ area\ C8 - C16}{Total\ \%area} xLiquid\ product\ (wt\%) \quad (6)$$

$$Diesel\ fraction = \frac{\%compound\ area\ C13 - C17}{Total\ \%area} xLiquid\ product\ (wt\%) \quad (7)$$

3. Results and Discussion

3.1. Characterization of PP, Ni(A)/PP, and Ni (B)/PP Catalysts

Figures 1 and 2 depict the FTIR spectra of the catalyst material before and after the acid test, which were performed to determine the functional groups present. Figure 1 shows the FTIR spectra of PP, Ni(A)/PP, and Ni catalysts. (B)/PP was recorded in the absorption area of 400-4000 cm^{-1}. The peak vibration at wavenumber 465 cm^{-1} includes the vibration of the Si–O–Si cyclosan group. At wavenumber 1080 cm^{-1} is the absorption peak of the asymmetric stretching vibration of the Si–O–Si group, wavenumber 1635 cm^{-1} is the z peak of the bending vibration of Si–OH, and at wavenumber 3455 cm^{-1} which is included in the stretching vibration of Si–OH [8,9]. Figure 2 depicts the FTIR spectrum of the interaction test results between the catalyst and pyridine molecules in the absorption region of 1350-700 cm^{-1}. Visible peak vibrations at the wavenumber region of 1460 cm^{-1} are associated with the coordination of pyridine bonds with Lewis acid sites [10-12]. At the wavenumber of 1635 cm^{-1}, an absorption peak is also seen, indicating the Brönsted-Lowry acid site, indicating a characteristic hydrogen-pyridine bond [13].

Figure 3 depicts the N_2 gas desorption adsorption isotherm curves for PP, Ni(A)/PP, and Ni(B)/PP catalysts. Figure 3 depicts two types of desorption adsorption isotherm curves, specifically, type I on microporous PP catalyst and type IV on Ni(A)/PP and Ni(B)/PP catalysts that exhibit mesoporous properties [14]. The type of hysteresis loop can also be identified based on the isotherm graph. The hysteresis

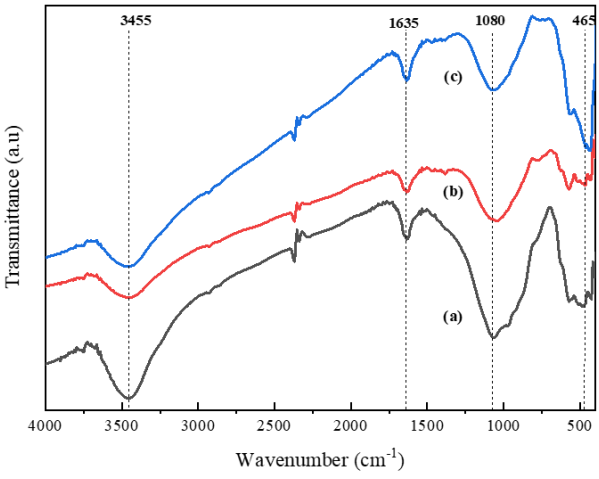

Figure 1. FTIR spectra of catalyst: (a) PP, (b) Ni(A)/PP, (c) Ni(B)/PP

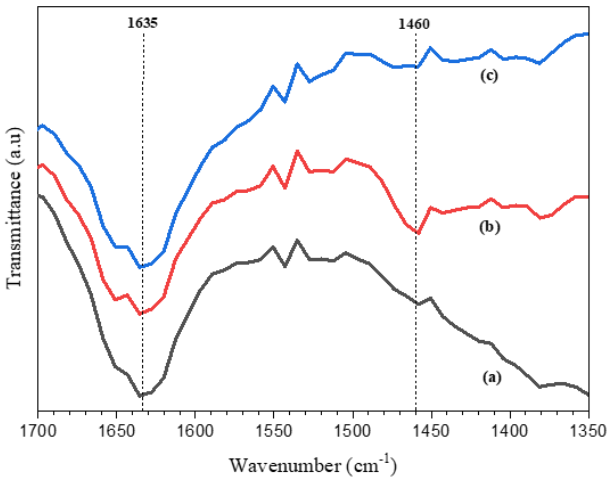

Figure 2. FTIR spectra after acid catalyst test: (a) PP, (b) Ni(A)/PP, (c) Ni(B)/PP

pattern of each catalyst shows the H4 type, which means that the pores on the catalyst are in the form of narrow slit pores [15]. Figure 4 depicts the distribution of the predominant pore size for each catalyst. Figure 4 illustrates the distribution of the dominant pore size on the PP, Ni(A)/PP, and Ni(B)/PP catalysts resulting in pores with a diameter of 2 nm. The pore distribution increased after the addition of Ni metal. This causes the average pore diameter of the catalyst after the addition of Ni metal to increase in the range of 2-50 nm. In this case, Ni(A)/PP and Ni(B)/PP catalysts have microporous and mesopore hierarchies. Figure 4 also reveals that the PP catalyst's pore distribution has a narrower peak range than that of the Ni(A)/PP and Ni(B)/PP catalysts, indicating that the PP catalyst is more homogeneous. The metal addition process produces a catalyst with a wider pore distribution and an increase in the optimum pore distribution on the catalyst [16]. This explains how the increase in pore size and formation of more heterogeneous pores are brought about by the addition of Ni metal to the sand surface.

Figure 5 displays the XRD crystallinity analysis results for PP, Ni(A)/PP, and Ni(B)/PP catalyst materials. The impregnation process of Ni metal on the Parangtritis beach sand carrier was successfully carried out. This is indicated by the presence of diffraction peaks that appear at 2θ = 43.6 and 2θ = 50.6 (JCPDS card no. 96-901-3034). There are also peaks at 2θ = 37 and 2θ = 62.5, which are characteristic of NiO (JCPDS card no. 96-432-0506). The presence of a NiO peak on the Ni(B)/PP catalyst is believed to be a result of its high Ni content, whereas the Ni(A)/PP catalyst lacks a NiO peak due to its lower Ni concentration [17].

Table 1 displays catalyst properties, including surface area, pore volume, average pore di-

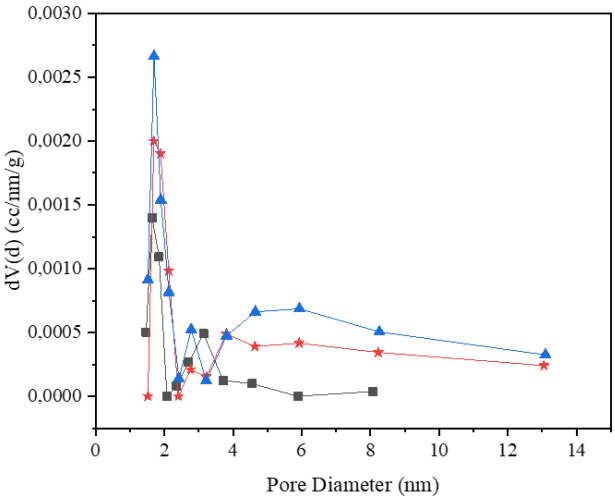

Figure 4. Pore distribution of catalyst (■) PP, (★) Ni(A)/PP, (▲) Ni(B)/PP

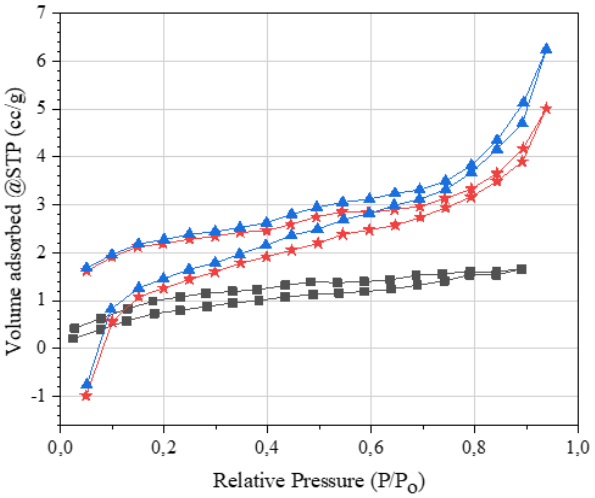

Figure 3. Catalyst isotherm graph: (■) PP, (★) Ni(A)/PP, (▲) Ni(B)/PP

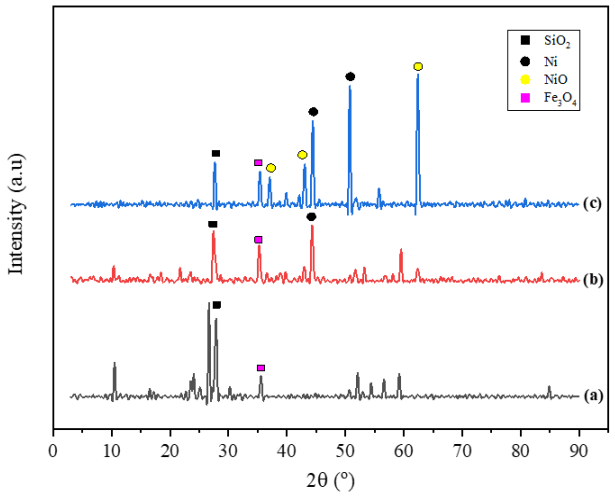

Figure 5. Catalyst diffraction: (a) PP, (b) Ni(A)/PP, and (c) Ni(B)/PP

Table 1. Catalyst properties

Catalyst	Surface area[a] (m^2/g)	Pore volume[a] (cc/g)	Average pore diameter[a] (nm)	Total acid amount[b] (mmol/g)	Metal loading[c] (wt%)	Crystal size (nm)
PP	3.43	0.0026	1.50	0.025	-	-
Ni(A)/PP	4.44	0.0078	3.50	0.051	6.55	25.86
Ni(B)/PP	4.47	0.0097	4.34	0.076	11.87	34.17

[a]Surface area, pore volume, and average pore diameters were determined using BET and BJH theory, [b]Total acid amount was determined by gravimetric method, [c]Metal loading was determined by using Energy Dispersive X-Ray (EDX).

ameter, total acidity, and metal concentration. Table 1 shows the change in the average pore diameter before and after metal impregnation from initially having microporous pores of 1.5 nm to 3.50 and 4.34 nm. An increase in the average pore diameter is followed by an increase in surface area. Normally, an increase in pore size causes a decrease in surface area. This is due to the uneven distribution of metal on the surface of the carrier as well as differences in pore size distribution [18]. The difference in pore size distribution results from the calcination, oxidation, and reduction processes performed on the catalyst, which restructured the solids' pores [19]. Changes in metal-carrier interactions during calcination, oxidation, and reduction lead to alterations in metal particle size, metal distribution, and pore size distribution in solid heterogeneous catalysts, according to [20]. The results indicated that the addition of metallic Ni increased the acidity value from Lewis acid site on the transition metal, with the total acidity value of Ni/PP increasing as the concentration of Ni added to the PP increased [21]. The size of the Ni metal crystals on the catalyst was calculated using the Scherer equation [22]. The calculation of the crystal size based on the Scherer equation revealed that as the metal concentration increased, the crystal size of the catalyst increased. According to [23], the crystal size is affected by the metal impregnation process, the type of metal, and the metal concentration. The larger the crystal obtained, the greater the metal concentration [24,25]. This is because a higher metal concentration leads to clusters of metal ions [26].

The morphology of the PP, Ni(A)/PP, and Ni(B)/PP catalysts from the SEM analysis is shown in Figure 6. Before impregnation with Ni metal, the PP catalyst morphology consisted of varying granules of varying sizes. However, there was a morphological change in the form of cotton lumps after the Ni metal impregnation process, indicating agglomeration on the

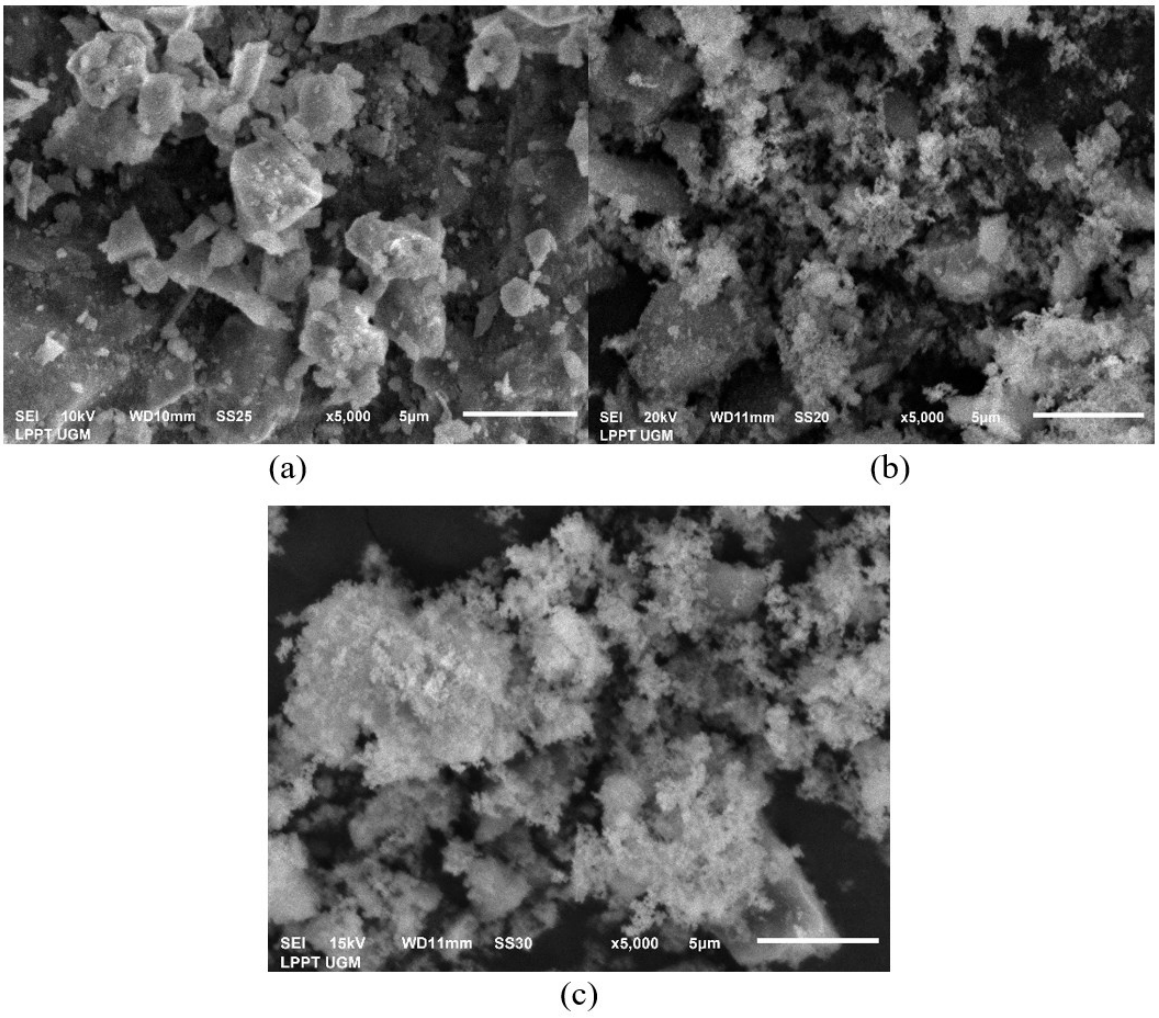

Figure 6. SEM images of catalysts: (a) PP, (b) Ni(A)/PP, (c) Ni(B)/PP

surface of the catalyst due to the addition of increasing concentrations of Ni and an uneven distribution of Ni [26]. Figures 6 (b) and (c) show the morphology of the catalyst with variations in the concentration of Ni metal. It can be seen that the higher the concentration of Ni metal, the greater the chance of agglomeration on the catalyst's surface [27]. Figure 7 depicts the distribution of Ni metal on the surface of the catalyst and verifies that Ni metal was successfully incorporated into the catalyst. It is also evident that the Ni(A)/PP catalyst has a more uniform distribution of Ni metal on the PP surface than the Ni(B)/PP catalyst. This is due to agglomeration events in which metal accumulates in specific areas.

3.2. Catalytic Activity and Selectivity Test

3.2.1 Catalytic activity and selectivity test of PP, Ni(A)/PP, dan Ni(B)/PP

The catalyst activity test was carried out through the hydrocracking process. Palm oil was the feed used in the catalyst activity test. Hydrocracking was performed at a temperature of 450 °C for 2 hours with a feed weight ratio of 1:200 while H_2 gas flowed at a rate of 20 mL/min. The catalyst with the highest activity was tested for reusability and used for hydrocracking in malapari oil. Table 2 displays the catalytic activity of the palm oil hydrocracking product.

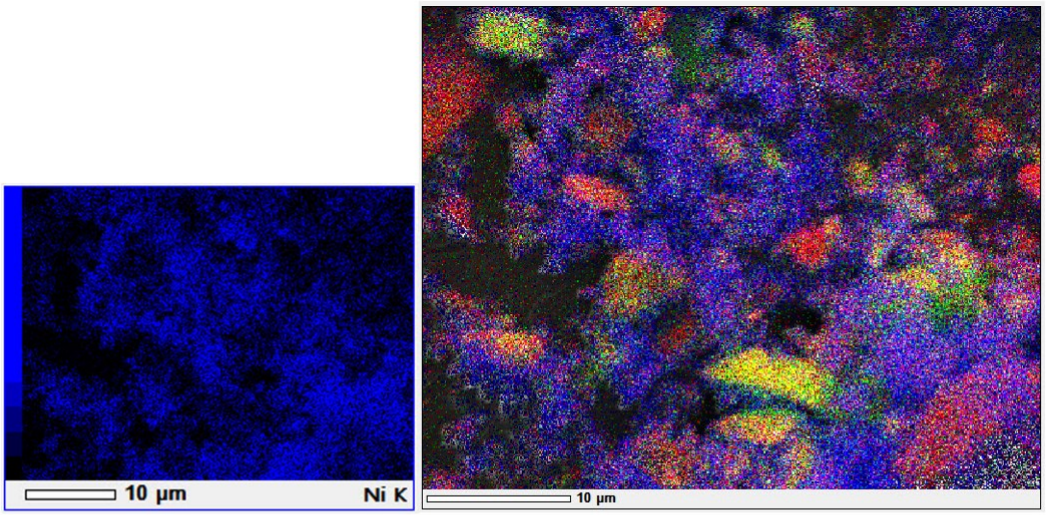

(a)

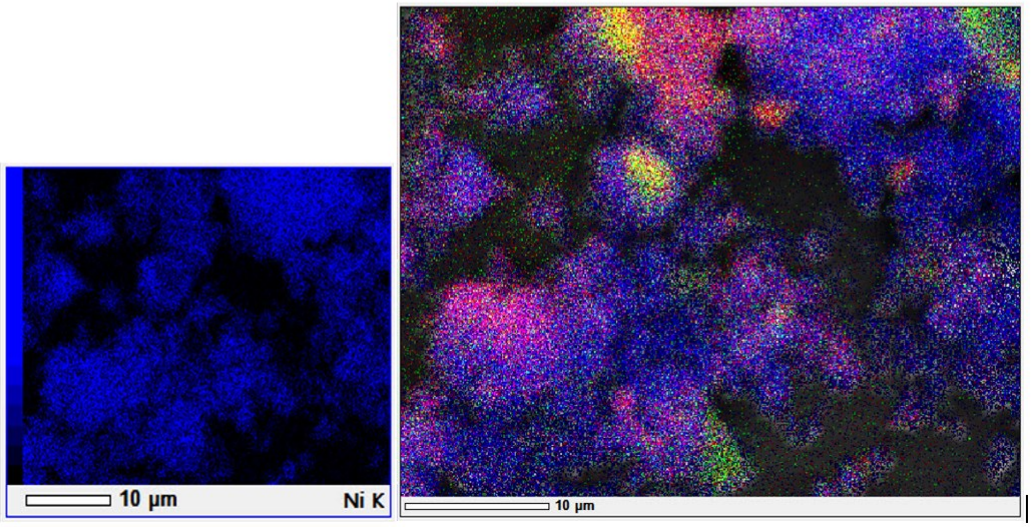

(b)

Figure 7. Distribution of Ni metal on the catalysts: (a) Ni(A)/PP, (b) Ni(B)/PP

The yield of the liquid product on the PP catalyst increased both before and after the Ni metal impregnation. This is because Ni metal has an active site that can assist in the hydrocracking process. The presence of unpaired electrons in the *d* orbitals causes an active site in Ni metal. Previous researcher [28] also stated that the total acidity value would increase after the metal impregnation process, which affects the increase of liquid products during the hydrocracking process. The catalyst with the highest liquid product yield was Ni(A)/PP, with a liquid product yield of 68.50 wt%, while the Ni(B)/PP catalyst had a higher acidity value than the Ni(A)/PP catalyst. It is believed that this is due to the uneven distribution of Ni metal on the Ni(B)/PP catalyst, which causes clumping at a specific location [29]. The surface of the catalyst pores is covered by clumping or uneven metal distribution, resulting in suboptimal catalyst conversion. This study conducted the catalyst selectivity test using GC-MS characterization. The results of GC-MS characterization show the compound fractions in the liquid product obtained from hydrocracking products, such as the hydrocarbon fraction, which is classified as biofuel fraction and other compounds. The fuel oil fraction consists of biogasoline (C_5-C_{12}), bioavtur (C_8-C_{16}), and biodiesel fraction (C_{13}-C_{18}) [30,31,32]. Figure 8 depicts the distribution of biohydrocarbons in the liquid product resulting from the hydrocracking of palm oil for each catalyst.

Figure 8 demonstrates that the Ni(A)/PP catalyst has the highest selectivity with fractions of 49.61 and 49.06 wt% for gasoline and avtur, respectively. This is supported by the XRD findings that the Ni(A)/PP catalyst contains no metal oxide (Ni^0). Unlike the Ni(B)/PP catalyst, which still contains a metal oxide, this catalyst does not contain metal oxide (NiO). Metal Ni^0 plays a crucial role in the hydrodeoxygenation process. The presence of zero metal (Ni^0) can prepare *d* orbitals containing a

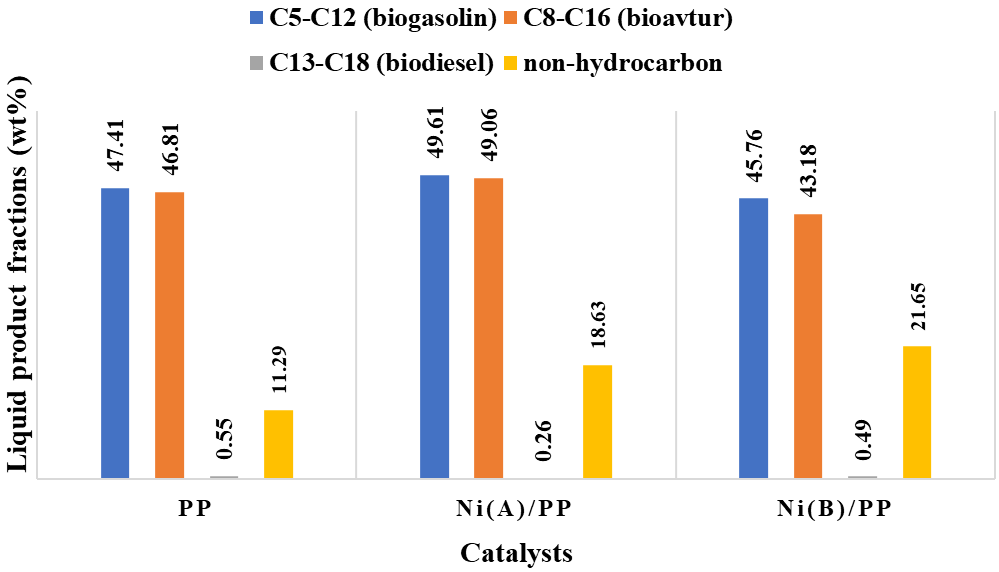

Figure 8. Distribution of biohydrocarbons in the liquid product resulting from hydrocracking of palm oil

Table 2. Hydrocracking products of palm oil

Hydrocracking conditions/ Catalyst	Conversion (wt%)				Total conversion (wt%)
	Liquid product	Gas product	Residue	Coke	
Thermal	50.25	29.10	20.65	0	79.35
PP	59.25	11.45	29	0.3	71.00
Ni(A)/PP	68.50	20.30	11.1	0.1	88.90
Ni(B)/PP	67.90	30.04	1.76	0.3	98.24

single electron to dissociate hydrogen homolytically, thereby optimizing the hydrodeoxygenation process [33-35]. Furthermore, the Ni(A)/PP catalyst, which has the highest activity and selectivity in the hydrocracking of palm oil, was tested for reusability and used in the hydrocracking process of malapari oil.

3.2.2 Reusability test of Ni(A)/PP

Stability and reusability tests were carried out on the Ni(A)/PP catalyst for 3 continuous runs using the used catalyst for two hours each at a temperature of 450 °C with a catalyst:feed ratio of 1:200 (w/w). Table 3 displays the activity of the catalyst on the stability and reusability test of the Ni(A)/PP catalyst. Table 3 shows that the hydrocracking process generally results in a less significant reduction in the liquid product. The decrease in the production of this liquid product can be attributed to the increase in coke formation after the third use, as shown in Table 3. Increasing the amount of coke further covers the catalyst's surface, which can block the access of molecules to the active site, so the hydrocracking process is not optimal [36]. The results of the selectivity test are shown in Figure 9. Overall, the activity and selectivity of the Ni(A)/PP catalyst indicated that it could produce biofuel fraction compounds from hydrocracked palm oil even after repeated use.

3.2.3 Test activity and selectivity of Ni(A)/PP catalyst on hydrocracking of malapari oil

The hydrocracking of malapari oil was conducted to evaluate further the activity and selectivity of the Ni(A)/PP catalyst, which exhibited the highest activity and selectivity in the hydrocracking of palm oil. Table 4 displays the results of the Ni(A)/PP catalyst activity test on the hydrocracking of malapari oil. Table 4 shows that the Ni(A)/PP catalyst for hydrocracking of malapari oil has almost the same activity as hydrocracking of palm oil. The

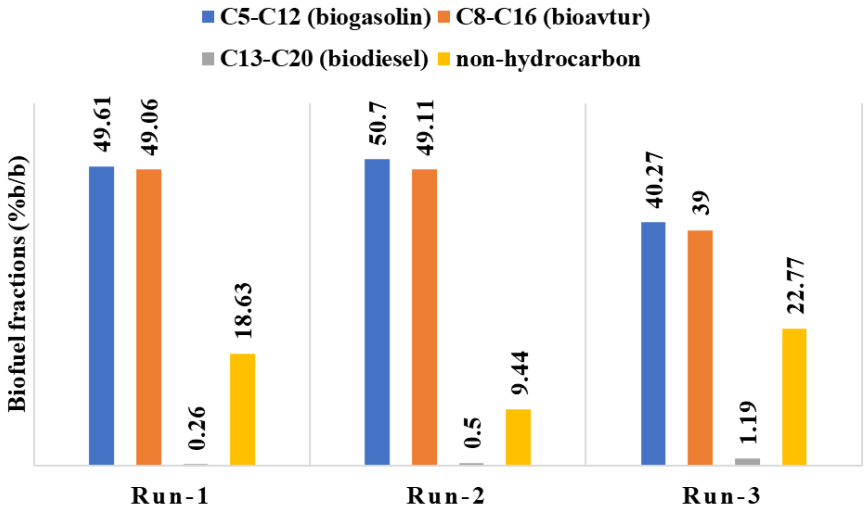

Figure 9. Graph of biofuel fraction products from the reusability tests using a Ni(A)/PP catalyst

Table 3. Palm oil hydrocracking reusability test product

Hydrocracking conditions/ Catalyst	Conversion (wt%)				Total conversion (wt%)
	Liquid product	Gas product	Residue	Coke	
Ni(A)/PP[1]	68.50	20.30	11.10	0.1	88.90
Ni(A)/PP[2]	60.65	20.05	19.10	0.2	80.90
Ni(A)/PP[3]	64.20	26.10	9.1	0.6	90.90

Table 4. Hydrocracking products of malapari oil

Feed (Oil)	Conversion (wt%)				Total conversions (wt%)
	Liquid product	Gas product	Residue	Coke	
Malapari	66.10	17.50	15.75	0.65	84.25

percentage of liquid product in malapari oil hydrocracking is less than the liquid product from palm oil hydrocracking. This decrease in the percentage of liquid product is likely due to the formation of more coke during the hydrocracking of malapari oil, resulting in a less optimal hydrocracking process. Figure 10 displays the results of the GC-MS characterization selectivity test. It can be seen that the biohydrocarbon fraction's selectivity in malapari oil's hydrocracking has the same selectivity in the hydrocracking of palm oil.

3.2.4 Catalyst morphology before and after palm oil hydrocracking

The morphology of PP, Ni(A)/PP, and Ni(B)/PP catalysts before and after hydrocracking of palm oil into biofuel was characterized using TEM. Figure 11 depicts the results of TEM analysis, indicating a change in color for each catalyst after use in the hydrocracking process. The catalyst's surface becomes darker due to the formation of coke, which covers its surface.

4. Conclusion

The total acidity, surface area, average pore diameter, and pore volume of PP catalyst are 0.025 mmol/g, 3.43 m^2/g, 1.50 nm, and 0.0026 cm^3/g, respectively. The impregnation of Ni metal into the sand catalyst improves the surface area, average pore diameter, and pore volume characteristics. Meanwhile, Ni(A)/PP catalyst possessed total acidity, surface area, average pore diameter, pore volume, and crystal size of 0.051 mmol/g, 4.44 m^2/g, 3.50 nm, 0.0078 cm^3/g, and 25.86 nm, respectively, Ni(B)/PP catalyst possessed 0.076 mmol/g, 4.47 m^2/g, 4.34 nm, 0.0097 cm^3/g, and 34.17 nm, respectively. Ni(A)/PP catalyst has the best activity and selectivity in the hydrocracking process of palm oil and malapari into biofuel. The liquid product yield and total biofuel fraction obtained from the hydrocracking of palm oil and malapari were 68.50, 49.87 wt% and 66.10, 47.83 wt%, respectively. The use of Ni(A)/PP catalyst repeatedly for 3 times shows that the catalyst has good stability. The liquid product yield and the total biofuel fraction obtained after the third use were 64.20 and 41.46 wt%, respectively.

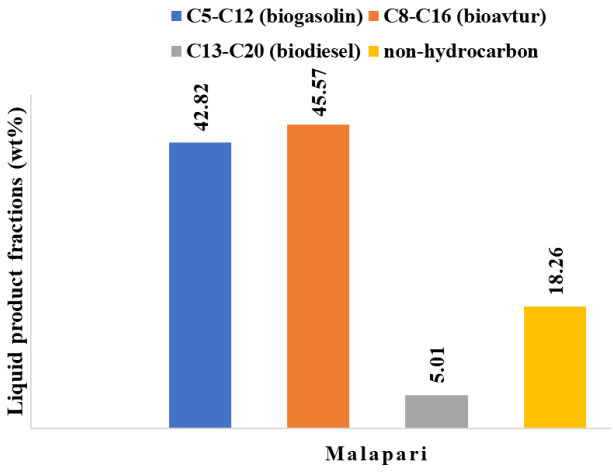

Figure 10. Distribution of biohydrocarbons in liquid product from hydrocracking of malapari oil

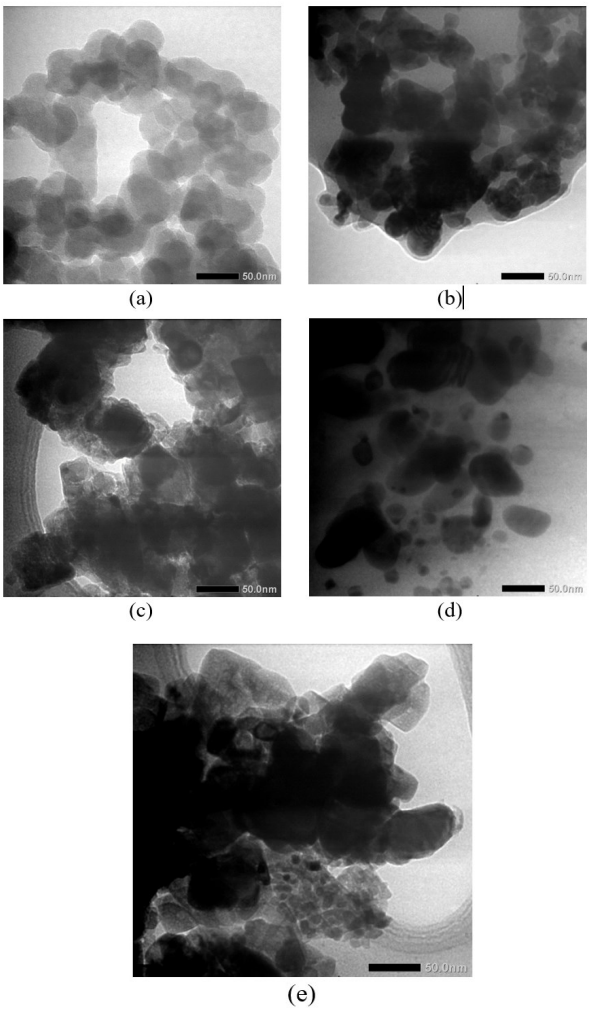

Figure 11. Catalyst morphology: (a) PP before hydrocracking, (b) PP after hydrocracking, (c) Ni(A)/PP before hydrocracking, (d) Ni(A)/PP after 3rd hydrocracking, (e) Ni (B)/PP before hydrocracking

Acknowledgement

This research was supported by LPDP (*Lembaga Pengelola Dana Pendidikan*), Ministry of Finance, Republic of Indonesia, through the Indonesian Education Scholarship program 2022.

References

[1] Talib, N.B., Triwahyono, S., Jalil, A.A., Mamat, C.R., Salamun, N., Fatah, N.A.A., Sidik, S.M., Teh, L.P. (2016). Utilization of a Cost Effective Lapindo Mud Catalyst Derived from Eruption Waste for Transesterification of Waste Oil. *Journal of Energy Conversion and Management*, 108, 411-421. DOI: 10.1016/j.enconman.2015.11.031

[2] Nanda, S., Rana, R., Hunter, H.N., Fang, Z., Dalai, A.K., Kozinski, J.A. (2019). Hydrothermal Catalytic Processing of Waste Cooking Oil for Hydrogen-Rich Syngas Production. *Chemical Engineering Science*, 195, 935-945. DOI: 10.1016/j.ces.2018.10.039

[3] Sentanuhady, J., Hasan, W.H., Muflikhun, M.A. (2022). Recent Progress on the Implementation of Renewable Biodiesel Fuel for Automotive and Power Plants: Raw Materials Perspective. *Advances in Materials Science and Engineering*, 2022, 19. DOI: 10.1155/2022/5452942

[4] Khowatimy, F.A., Priastomo, Y., Febriyanti, E., Riyantoko, H., Trisunaryanti, W. (2014). Study of Waste Lubricant Hydrocracking into Fuel Fraction over the Combination of Y-Zeolite and ZnO Catalyst. *Procedia Environmental Sciences*, 20, 225-234. DOI: 10.1016/j.proenv.2014.03.029

[5] Cao, X., Li, L., Shitao, Y., Liu, S., Hailong, Y., Qiong, W., Ragauskas, A.J. (2019). Catalytic Conversion of Waste Cooking Oils for the Production of Liquid Hydrocarbon Biofuels Using In-Situ Coating Metal Oxide on SBA-15 as Heterogeneous Catalyst. *Journal of Analytical and Applied Pyrolysis*, 138, 137-144. DOI: 10.1016/j.jaap.2018.12.017

[6] de Oliveira, K.G., de Lima, R.R., de Longe, C., Bicudo, T.D.C., Sales, R.V., de Carvalho, L.S. (2022). Sodium and Potassium Silicate-Based Catalysts Prepared Using Sand Silica Concerning Biodiesel Production from Waste Oil. *Arabian Journal of Chemistry*, 15, 103603. DOI: 10.1016/j.arabjc.2021.103603

[7] Alisha, G.D., Trisunaryanti, W., Syoufian, A. (2022). Hydrocracking of Waste Palm Cooking Oil into Hydrocarbon Compounds over Mo Catalyst Impregnated on SBA-15. *Silicon*, 14, 2309-2315. DOI: 10.1007/s12633-021-01035-1

[8] Chen, L., Hu, J., Qi, Z., Fang, Y., Richards, R. (2011). Gold Nanoparticles Intercalated into the Walls of Mesoporous Silica as a Versatile Redox Catalyst. *Industrial & Engineering Chemistry Research*, 50, 13642-13649. DOI: 10.1021/ie200606t

[9] Ghosh, B.K., Hazra, S., Naik, B., Ghosh, N.N. (2015). Preparation of Cu Nanoparticle Loaded SBA-15 and Their Excellent Catalytic Activity in Reduction of Variety of Dyes. *Powder Technology*, 269, 371-378. DOI: 10.1016/j.powder.2014.09.027

[10] Yiu, H.H.P., Brown, D.R. (1998). Lewis and Brønsted Acid Catalysis with AlMCM-41 and AlMMS: Dependence on Exchange Cation. *Catalysis Letters*, 56, 57-64. DOI: 10.1023/A:1019040508711

[11] Platon, A., Thomson, W.J. (2003). Quantitative Lewis/Brönsted Ratios Using Drifts. *Industrial & Engineering Chemistry Research*, 42, 5988-5992. DOI: 10.1021/ie030343g

[12] Naik, S.P., Chiang, A.S., Thompson, R.W. (2003). Synthesis of Zeolitic Mesoporous Materials by Dry Gel Conversion Under Controlled Humidity. *The Journal of Physical Chemistry B*, 107, 7006-7014. DOI: 10.1021/jp034425u

[13] Tanabe, K. (1981). *Solid Acid and Base Catalyst in Catalysis Science and Technology*. John R Anderson and Michael Boudart (eds) Vol. 2, Springer-Link Berlin, 231-273.

[14] Alothman, Z.A. (2012). A Review: Fundamental Aspects of Silicate Mesoporous Materials. *Materials*, 5, 2874-2902. DOI: 10.3390/ma5122874

[15] Dong, H., Liu, Q. (2020). Three-Dimensional Networked Ni-Phyllosilicate Catalyst for CO_2 Methanation: Achieving High Dispersion and Enhanced Stability at High Ni Loadings. *ACS Sustainable Chemistry & Engineering*, 8, 6753-6766. DOI: 10.1021/acssuschemeng.0c01148

[16] Ancheyta, J., Rana, M.S., Furimsky, E. (2005). Hydroprocessing of Heavy Petroleum Feeds: Tutorial. *Catalysis Today*, 109, 3-15. DOI: 10.1016/j.cattod.2005.08.025

[17] Tang, C., Li, J., Yao, X., Sun, J., Cao, Y., Zhang, L., Gao, F., Deng, Y., Dong, L. (2015). Mesoporous NiO–CeO_2 Catalysts for CO Oxidation: Nickel Content Effect and Mechanism Aspect. *Applied Catalysis A: General*, 494, 77-86. DOI: 10.1016/j.apcata.2015.01.037

[18] Yang, Y., Ochoa-Hernández, C., Víctor, A., Pizarro, P., Coronado, J.M., Serrano, D.P. (2014). Effect of metal–support interaction on the selective hydrodeoxygenation of anisole to aromatics over Ni-based catalysts. *Applied Catalysis B: Environmental*, 145, 91-100. DOI: 10.1016/j.apcatb.2013.03.038

[19] Serrano, D.P., Sanz, R., Pizarro, P., Moreno, I., Shami, S. (2014). Narrowing the Mesopore Size Distribution in Hierarchical TS-1 Zeolite by Surfactant-Assisted Reorganization. *Microporous and Mesoporous Materials*, 189, 71-82. DOI: 10.1016/j.micromeso.2013.09.020

[20] Zhang, G., Sun, Y., Xu, Y., Zhang, R. (2018). Catalytic Performance of N-Doped Activated Carbon Supported Cobalt Catalyst for Carbon Dioxide Reforming of Methane to Synthesis Gas. *Journal of the Taiwan Institute of Chemical Engineers*, 93, 234-244. DOI: 10.1016/j.jtice.2018.07.016

[21] Hernando, H., Moreno, I., Fermoso, J., Ochoa-Hernández, C., Pizarro, P., Coronado, J.M., Čejka, J. and Serrano, D.P. (2017). Biomass Catalytic Fast Pyrolysis over Hierarchical ZSM-5 and Beta Zeolites Modified with Mg and Zn Oxides. *Biomass Conversion and Biorefinery*, 7, 289-304. DOI: 10.1007/s13399-017-0266-6

[22] Niemantsverdriet, J.W. (2007). *Spectroscopy in* catalysis*: an introduction*. John Wiley & Sons.

[23] Santi, D., Trisunaryanti, W., Falah, I.I. (2020). Hydrocracking of Pyrolyzed α-Cellulose to Hydrocarbon over MxOy/Mesoporous Carbon Catalyst (M= Co and Mo): Synthesis and Characterization of Carbon-Based Catalyst Support from Saw Waste of Merbau Wood. *Journal of Environmental Chemical Engineering*, 8, 103735. DOI: 10.1016/j.jece.2020.103735

[24] Dong, W., Mansour, A.N., Dunn, B. (2001). Structural and Electrochemical Properties of Amorphous and Crystalline Molybdenum Oxide Aerogels. *Solid State Ionics*, 144, 31-40. DOI: 10.1016/S0167-2738(01)00901-8

[25] Dhar, G.M., Kumaran, G.M., Kumar, M., Rawat, K.S., Sharma, L.D., Raju, B.D., Rao, K.R. (2005). Physico-Chemical Characterization and Catalysis on SBA-15 Supported Molybdenum Hydrotreating Catalysts. *Catalysis Today*, 99, 309-314. DOI: 10.1016/j.cattod.2004.10.005

[26] Botas, J.A., Serrano, D.P., García, A., De Vicente, J., Ramos, R., 2012, Catalytic Conversion of Rapeseed Oil into Raw Chemicals and Fuels over Ni- and Mo-Modified Nanocrystalline ZSM-5 Zeolite. *Catalysis Today*, 195, 59-70. DOI: 10.1016/j.cattod.2012.04.061

[27] Millet, M.M., Algara-Siller, G., Wrabetz, S., Mazheika, A., Girgsdies, F., Teschner, D., Seitz, F., Tarasov, A., Levchenko, S.V., Schlögl, R., Frei, E. (2019). Ni Single Atom Catalysts for CO_2 Activation. *Journal of the American Chemical Society*, 141, 2451-2461. DOI: 10.1021/jacs.8b11729

[28] Trisunaryanti, W., Larasati, S., Bahri, S., Ni'mah, Y.L., Efiyanti, L., Amri, K., Nuryanto, R., Sumbogo, S.D. (2020). Performance Comparison of Ni-Fe Loaded on NH_2-Functionalized Mesoporous Silica and Beach Sand in the Hydrotreatment of Waste Palm Cooking Oil. *Journal of Environmental Chemical Engineering*, 8, 104477. DOI: 10.1016/j.jece.2020.104477

[29] Osgood, H., Devaguptapu, S.V., Xu, H., Cho, J., Wu, G. (2016). Transition metal (Fe, Co, Ni, and Mn) oxides for oxygen reduction and evolution bifunctional catalysts in alkaline media. *Nano Today*, *11*(5), 601-625. DOI: 10.1016/j.nantod.2016.09.001

[30] Istadi, I., Buchori, L., Anggoro, D.D., Riyanto, T., Indriana, A., Khotimah, C., Setiawan, F.A.P. (2019). Effects of ion exchange process on catalyst activity and plasma-assisted reactor toward cracking of palm oil into biofuels. *Bulletin of Chemical Reaction Engineering & Catalysis*, 14, 459-467. DOI: 10.9767/bcrec.14.2.4257.459-467

[31] Blakey, S., Rye, L., Wilson, C.W. (2011). Aviation Gas Turbine Alternative Fuels: A Review. *Proceedings of The Combustion Institute*, 33, 2863-2885. DOI: 10.1016/j.proci.2010.09.011

[32] Nugrahaningtyas, K.D., Lukitawati, R., Mukhsin, S.A., Fadlulloh, Z., Sabiilagusti, A.I., Budiman, A.W., Kurniawati, M.F. (2022, March). Conversion of waste cooking oil into green diesel using Ni/MOR and Cu/MOR catalysts. In *Journal of Physics: Conference Series* (Vol. 2190, No. 1, p. 012037). IOP Publishing.

[33] Ameen, M., Azizan, M.T., Ramli, A., Yusup, S., Abdullah, B. (2020). The Effect of Metal Loading Over Ni/Γ-Al_2O_3 and Mo/Γ-Al_2O_3 Catalysts on Reaction Routes of Hydrodeoxygenation of Rubber Seed Oil for Green Diesel Production. *Catalysis Today*, 355, 51-64. DOI: 10.1016/j.cattod.2019.03.028

[34] Kusumastuti, H., Trisunaryanti, W., Falah, I.I., Marsuki, M.F. (2018). Synthesis of Mesoporous Silica-Alumina from Lapindo Mud as a Support of Ni and Mo Metals Catalysts for Hydrocracking of Pyrolyzed α-cellulose. *Rasayan J. Chem.*, 11, 522-530. DOI: 10.31788/RJC.2018.1122061

[35] Zhao X, Wei L, Cheng S, Kadis E, Cao Y, Boakye E, Gu Z, Julson J (2016) Hydroprocessing of carinata oil for hydrocarbon biofuel over Mo-Zn/Al_2O_3. *Applied Catalysis B: Environmental*, 196, 41–49. DOI: 10.1016/j.apcatb.2016.05.020

[36] Absi-Halabi, M., Stanislaus, A., Trimm, D L. (1991). Coke formation on catalysts during the hydroprocessing of heavy oils. *Applied Catalysis*, 72, 193-215. DOI: 10.1016/0166-9834(91)85053-X